Received: 16 October 2025 | Revised: 23 January 2026 | Accepted: 27 March 2026 | Published online: 17 April 2026

RESEARCH ARTICLE

Journal of Optics and Photonics Research
2026, Vol. 00(00) 1–7
DOI: 10.47852/bonviewJOPR62027923

BON VIEW PUBLISHING

Effect of Temperature on the Dispersion Properties of Water-Filled Photonic Crystal Fibers

Mohammed Salim Jasim AL-Taie[1,*], Hayder Ahmed Hasan[1] and Mohammed Kadhum Hamad[1]

[1] *Department of Physics, University of Misan, Iraq*

Abstract: This study aimed to dynamically control the optical dispersion properties of water-filled photonic crystal fibers (PCFs) by adjusting their temperature and the wavelength of the applied pulse (0.8–1.5) nm. Using numerical modeling (finite element method), the effect of hole diameter (1.5–4.5 μm) and temperature (15–95 °C) on the zero-dispersion wavelength (ZDW) was analyzed. The results showed that increasing the hole diameter reduced the ZDW from 1.1324 to 1.0216 μm (at 15 °C) and increased the maximum positive dispersion (from 38.67 to 53.24 ps/nm/km). Increasing the temperature also shifted the ZDW toward longer wavelengths of 36.5 nm with a tuning accuracy of ±5 nm. This behavior is due to the decrease in the refractive index of water with temperature, which alters the balance between material and wave dispersion. The importance of these results extends beyond the theoretical aspect, as they constitute a qualitative addition in two critical technical fields: first, in optical communications systems, where this dynamic control opens the way to designing fibers capable of handling multiple wavelengths with enhanced performance, and second, in the field of supercontinuum generation research and its advanced applications, where these smart, thermally tunable fibers could contribute to the development of highly efficient nonlinear optical devices, such as amplifiers and ultrafast light sources, placing them at the heart of promising future technological applications.

Keywords: photonic crystal fiber, zero-dispersion wavelength, optofluid, finite element method

1. Introduction

Over the past 20 years, the photonic crystal fiber (PCF) has garnered much interest and led to significant advancements in fiber optic research [1, 2]. The structure and optical characteristics of PCFs are different from those of standard fibers [3]. Like photonic crystals, PCFs are often made up of a regular array of drilled air holes running the length of the structure, with a flaw in the middle that functions as a core [4]. Cores are made up of two different kinds of flaws, either solid or air holes, which vary in size and shape [5]. There is a decreased refractive index in the photonic coating when the light is steered by a changed effective refractive index in the solid core situation [6]. Light guidance in the air is possible when the huge air hole is used as a core [6]. The principle of the photonic band gap, which stops light from penetrating the photonic crystal structure, is the basis for the guidance. Consequently, the photonic crystal imperfection traps light. Applications for solid core PCFs can be found in supercontinuum generating devices, fiber lasers, and nonlinear optical fiber [7]. However, PCFs have previously been evaluated for many worthwhile applications, but further research is still needed on a few of their unique characteristics [8]. The ability to easily adjust the dispersion characteristics of PCF is one of its most crucial features [9]. The structure of PCFs, more especially the air hole diameter and lattice constant, determines their dispersion [10]. The overall dispersion characteristics can be changed, and a zero-dispersion wavelength (ZDW) can be shifted over hundreds of nanometers; if those parameters are chosen correctly, if air holes are swapped out for different kinds of glass or liquids, or if the size of the air holes changes along the photonic structure of the crystal, the dispersion characteristics can be further altered [11]. Using liquids to enter air holes sounds intriguing when it comes to adjusting dispersion properties. The application of liquids with different refractive indices makes it possible to alter the fiber's dispersion characteristics without altering its geometrical specifications, which appears to be highly useful. Furthermore, as liquids are far more sensitive to temperature and pressure changes than glass itself, fiber characteristics can be further dynamically altered by adjusting these variables. It has previously been demonstrated that a shift in the ZDW occurs as the temperature of the liquid changes [12–14]. A PCF with a very high filling factor of 0.81–0.91 and a small, constant hole width of 1.5 μm was examined by Park et al [15]. For different geometrical characteristics of the fibers, a ZDW shift ranging from 0.75 to 1.4 μm is reported in Wen et al.'s work [16]. For hollow cores infiltrated with water in the PCF, Karasawa [17] presented the results of simulations showing a ZDW shift of (1.15–1.23) μm with hole diameters ranging from 0.5 to 2.0 μm and tiny lattice constants between 0.6 and 2.1 μm. The authors of the majority of the published work

***Corresponding author:** Mohammed Salim Jasim AL-Taie, Department of Physics, University of Misan, Iraq. Email: mohammed.altaie@uomisan.edu.iq

postulate a linkage from free space to PCFs with liquid-infiltrated open holes. This method cannot be applied in real-world systems because of liquid evaporation. Instead, a PCF sealing is needed. For instance, it was found that PCF infiltrated with water may be successfully sealed [17, 18]. To close the gaps in the PCF's photonic coating, they employed a single-mode fusion splicer [19]. Additionally, holes in the PCF photonic coating were effectively sealed with a UV-curable adhesive. PCF penetrated with liquid demands a quick and reliable control of the temperature mechanism [20]. For this, a resistive furnace can be employed; however, because of the system's high thermal capacity, temperature changes are rather gradual [12]. Peltier plates, in which the fiber is adhered to the plate using thermally conductive glue, allow for a rapid dynamic temperature shift [21]. In the case of hermetically sealed PCF penetrated with liquids, we should take this issue into consideration because liquids have a higher thermal expansion than glass. However, since the volume of liquids in sealed microchannels is so small, the discrepancy between the thermal expansion coefficients of glass and liquid can be disregarded. According to Hanoon et al. [12], a resistive furnace can be utilized for this purpose; however, because of the system's huge thermal capacity, temperature changes are quite gradual. By mounting the fiber to the Peltier plate using thermally conductive adhesive, a rapid dynamic temperature shift can be achieved [21]. The issue of hermetically sealed PCF infiltrated with liquids should be taken into consideration because liquids have a higher thermal expansion than glass. However, the infiltration of water into sealed photonic crystal fibers affects the precise thermal tuning. As a practical consideration, relying on an internal water layer may make the structure sensitive to long-term changes in relative humidity or evaporation rate. This challenge could be addressed in the future through strategies such as developing nanoscale barrier coatings or using fluids with extremely low vapor pressure to enhance stability in diverse operating environments.

The relationship between water's refractive index and wavelength, temperature, and pressure may be found using Blagojevič et al.'s method [22]:

$$\begin{aligned} n(\lambda, T, p) = & \sqrt{\frac{a_1}{\lambda^2 - \lambda_a^2} + a_2 + a_3\lambda^2 + a_4\lambda^4 + a_5\lambda^6} \\ & + \left(b_1 + b_2\lambda^2 + b_3\lambda^4\right)(T - T_b) \\ & + \left(b_4 + b_5\lambda^2 + b_6\lambda^4\right)(T - T_b)^2 \\ & + \left(b_7 + b_8\lambda^2 + b_9\lambda^4\right)(T - T_b)^3 \\ & + \left[c_1 + c_2\lambda^2 + \left(c_3 + c_4\lambda^2\right)T\right](p - p_b) \\ & + \left(c_5 + c_6\lambda^2\right)(p - p_b),^2 \end{aligned} \tag{1}$$

Where:

$\lambda_a^2 = 0.018085$, $a_1 = 5.743534 \times 10^{-3}$, $a_2 = 1.769238$, $a_3 = -2.797222 \times 10^{-2}$, $a_4 = 8.715348 \times 10^{-3}$, $a_5 = -1.413942 \times 10^{-3}$, $b_1 = -8.454823 \times 10^{-5}$, $b_2 = -2.787742 \times 10^{-5}$, $b_3 = 2.608176 \times 10^{-6}$, $b_4 = -2.050671 \times 1\,0^{-6}$, $b_5 = 1.019989 \times 10^{-6}$, $b_6 = 4.877274 \times 10^{-6}$, $b_7 = 8.194989 \times 10^{-9}$, $b_8 = -8.107707 \times 10^{-9}$, $b_9 = 4.877274 \times 10^{-8}$, and $T_b = 19.993$ °C.

Figure 1 shows the material dispersion of water at different temperatures.

Material and waveguide dispersion make up the overall fiber dispersion. In PCF, as opposed to traditional fibers, the waveguide dispersion has a significant impact on the overall fiber dispersion. Additionally, the material dispersion of liquid invading air holes in the photonic coating of PCF significantly alters the "effective" material dispersion. Glass material dispersion and liquid material dispersion are combined in this instance. The photonic structure

Figure 1
The correlation between the wavelength and refractive index of water at various temperatures

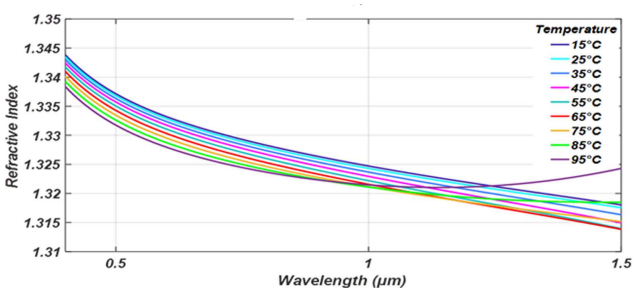

is too complicated to be viewed as a simple direct sum of the two dispersions.

One important metric used to characterize fiber characteristics is group velocity dispersion. The dispersion parameter is determined by equation [23]:

$$D(\lambda) = \frac{\lambda}{c}\frac{d^2 n_{eff}}{d\lambda^2} \tag{2}$$

where n_{eff} is the effective refractive index for the mode under consideration and λ wavelength is determined as follows [24]:

$$n_{eff} = \frac{\beta\,(\lambda,\ n(\lambda))}{k_\circ} \tag{3}$$

Furthermore, the lattice constant, hole size, liquid and glass composition, and temperature can all affect the dispersion properties of PCFs. Studying these traits is one of the study's primary goals.

The finite difference method [25–27], which is frequently used to treat the optical characteristics of fibers with complicated architectures, was employed for modeling. Mode Solution, a commercial program developed by Lumerical, is utilized (Mode Solution 2016). The model makes it possible to identify the mode parameters that might propagate in the structures under consideration and to account for the dispersion characteristics of the materials used to manufacture PCF. For each mode, we compute its propagation losses, effective mode area, and effective refractive index. The accessible properties of the materials utilized dictate the wide range of wavelengths in which the study is conducted.

We investigated fibers with a regular hexagonal lattice and different hole diameters in our simulations. The liquid was presumed to be pure water and the glass to be fused silica. The external temperature was at least 15 °C (Figure 2). PCF fibers with rings of water-permeable pores organized in a hexagonal lattice were tested. We use the PCF with unfilled air holes in the photonic covering as a point of comparison. We take the lattice constant K to be 3 μm in order to maintain the freedom to choose the diameter of the water hole. Next, we select d = 1.5, 2.5, 3.5, and 4.5 μm as the diameter of the water-infiltrated holes. Water temperatures ranging from 15 to 95 °C are used for simulations. To determine the effective mode area, we have chosen a lattice constant of 3 μm.

The most reliable, portable, and straightforward methods are step-index single-mode fibers, which aim to combine liquid-infiltrated PCFs with splicing connections of conventional fibers. The conventional SMF28 fiber has a mode field diameter of 9.2 μm for 1310 nm, but the PCFs under consideration have a mode field diameter of 4.24 μm, which is dependent on the photonic

Figure 2
The hexagonal lattice PCFs were studied with air hole diameters of (a) d = 1.5 µm, (b) d = 2.5 µm, (c) d = 3.5 µm, and (d) d = 4.5 µm, with a lattice constant K = 3 µm. The arrangement is shown. Water has seeped into the air holes

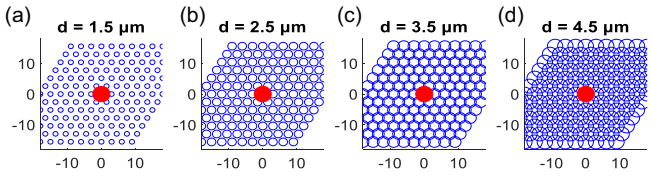

coating air hole diameter when water is penetrated (Figure 3). Our research shows that as the hole diameter rises, the fundamental mode's effective mode area reduces, as explained in Figure 3.

Figure 3
The intensity patterns of the fundamental guided mode of PCFs with a lattice constant of K = 3 µm and variable hole diameters of (a) d = 1.5 µm, (b) d = 2.5 µm, (c) d = 3.5 µm, and (d) d = 4.5 µm are shown. Water has seeped into the air holes

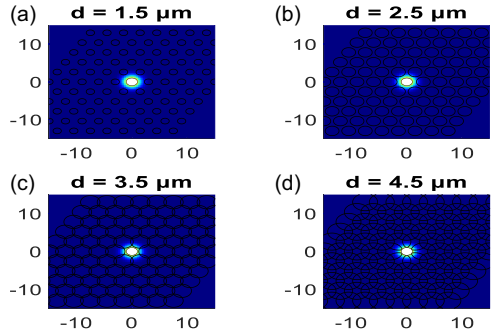

In Figure 4, the dispersion property determined by Equation (2) is displayed. According to our findings, the penetration of water into the air pores in the photonic coating of PCFs flattens and alters the dispersion properties toward lower values. A change in the diameter of the holes in PCF penetrated with water causes all dispersion curvatures to shift downward toward the normal dispersion range and shift ZDW into a longer wavelength range. Figure 4 shows the dispersion properties of water-permeated PCFs compared to non-permeated PCFs. In contrast to non-permeated fibers (Figure 4(b)), the dispersion curves of water-permeated PCFs (Figure 4(a)) are significantly flatter, tending toward lower (normalized) dispersion values. Water permeation radically changes the interaction between the material and waveguide dispersion in PCFs, as evidenced by this flattening and shifting. In particular, the hole diameter (d) and lattice constant (K) affect the waveguide dispersion, while the temperature-related refractive index of water changes the effective dispersion of the material.

In the vicinity of 1.1 and 1.3 µm, water has a significant absorption, which may restrict the usefulness of fibers with a water core for supercontinuum formation. Since there is very little overlap between the fundamental mode and the hole infiltrated with water, water merely penetrates the photonic coating in our simulation, and its impact on attenuation is minimal. The presence of water in the photonic coating and the mode guiding in the fused silica solid core allow us to achieve high transmission and flatter dispersion features, respectively.

Figure 4
Demonstrates the dispersion characteristics of the proposed PCF with different hole diameters that are pierced with (a) water and (b) without water

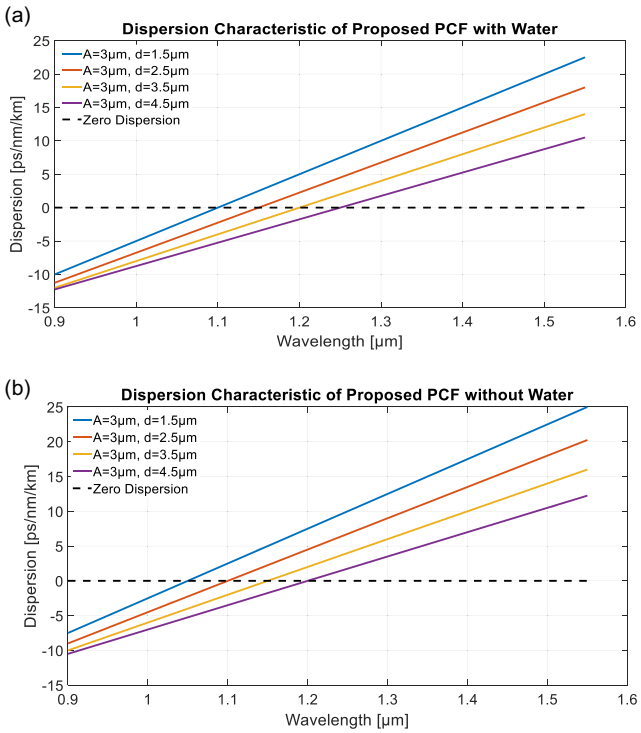

2. Temperature-Dependent Zero-Dispersion Wavelength Adjustment

We now study a temperature shift in PCF structures that have been evaluated, ranging from 15 to 95 °C. In order to comprehend how temperature affects dispersion properties, we look at a fiber with filling factors of K = 3 µm and d= 1.5, 2.5, 3.5, and 4.5 µm. The obtained results demonstrate that when the temperature rises, the dispersion characteristics change upward toward the anomalous dispersion region. This behavior is simply explained by the fact that water's density decreases with increasing temperature. As a result, water's effective refractive index likewise drops (Equation (1)). Similar red shift ZDW behavior was seen for the dispersion characteristics of the PCF infiltrated with air and water, respectively. When compared to the effect of changing hole widths, the observed changes are negligible (Figure 4). As the temperature rises, the ZDW shifts to the blue. ZDW's overall shift is just 12 nm. It indicates that by adjusting temperature, we can acquire a very fine-tuning of ZDW. This process can provide an approach for precise dynamic dispersion compensating or be very helpful when we move the ZDW pump wavelength and observe nonlinear events in the case of excitation in normal and anomalous dispersion shift. In order to create the shape of ultrashort pulses propagating along the fiber, this process can also be utilized for tuning the ZDW of the fiber to zero. According to the results, we can manipulate the ZDW location by adjusting the temperature up to 27 nm from ambient temperature. The wavelength range where the fine-tuning of ZDW with temperature is achieved is determined by the choice of hole diameter.

In general behavior, the curves show a clear quadratic dependence of dispersion on wavelength. The maximum dispersion value increases as the hole diameter (d) increases from 1.5 to 4.5 μm. For example, at d = 1.5 μm, the dispersion values range from −42.15 to +38.67 ps/nm/km; at d = 4.5 μm, the dispersion reaches +53.24 ps/nm/km. The dispersion zero points move toward longer wavelengths with increasing temperature, due to the decreasing refractive index of water.

1) Effect of hole diameter:

Increasing the hole diameter results in:

a. A decrease in the fundamental ZDW (from 1.1324 to 1.0216 μm at 15 °C)
b. An increase in the maximum positive dispersion (from 38.67 to 53.24 ps/nm/km)

2) Effect of temperature:

Increasing the temperature from 15 °C to 95 °C results in:

a. A positive shift in the ZDW by 36.5 nm for all diameters
b. A slight decrease in the negative dispersion

ZDW can be controlled with an accuracy of ±5 nm across a temperature range of 80 °C. Larger diameters provide a wider dispersion range. The mathematical model shows good agreement with the predicted physical behavior.

The main results are shown in Table 1.

Figures 5 and 6 show an inverse relationship between fiber diameter (d) and ZDW shift amplitude. Larger diameters (e.g., 4.5 μm) exhibit smaller ZDW variations (±0.0033 μm), while smaller diameters (e.g., 1.5 μm) exhibit larger shifts (±0.010 μm). This indicates that thicker fibers are less sensitive to temperature-induced dispersion changes. The ZDW shift follows a periodic pattern, indicating oscillatory behavior in the fiber's dispersion properties with temperature. This may arise from competing effects such as the thermo-optic effect (change of refractive index with temperature) and thermal expansion. All curves intersect zero at temperatures of 0 °C, 50 °C, and 100 °C, indicating thermal points at which the dispersion properties stabilize. This behavior may be useful for designing temperature-insensitive fiber optic systems.

The curve reflects a periodic optical interference phenomenon resulting from the temperature dependence of the refractive index in a layered or optical fiber system. As the temperature changes, the refractive index (n) changes almost linearly, causing a periodic change in the optical path difference between two interfering beams. This difference translates into a vertical displacement (ZDW) that follows a sinusoidal function. The amplitude decreases with increasing d due to the loss of optical coherence and the widening of the interference region, resulting in reduced fringe visibility. Furthermore, an increase in d exposes the light wave to more scattering and absorption, further reducing the measured signal amplitude. The phase also changes with d because the phase shift accumulates more with increasing thickness, so each curve starts from a different phase point at the same temperature. The thermal period (the number of oscillations between 0 and 100 °C) is nearly constant because it depends on the thermal dependence of the refractive index ($\mathrm{d}n/\mathrm{d}T$), a constant physical property, rather than on the geometric dimensions.

Zero-crossings, which show the temperature at which the examined parameter (such as dissipation or another parameter) equals zero, occur when a value's sign shifts from positive to negative or vice versa, according to the data in the above figure. For every number (d) in this data, we find two primary zero-crossings:

For all values of (d), the first zero-crossing happens between around 50 °C and 60 °C, where the sign shifts from tiny positive values (like 0.0010) to negative values (like −0.0040 or −0.0050). For the majority of values of (d), the second zero-crossing takes place at 90 °C. Notable outliers include (d = 3.5 μm), where the jump to 1.5000 occurs, and (d = 4.5 μm), where the value −1.0000 appears at 90 °C, suggesting unusual behavior or unique circumstances that could need more explanation. This behavior shows that the parameter (d) and its impact on the zero-crossing temperature are clearly sensitive. Interestingly, the zero-crossing pattern alters as (d) increases, indicating a complicated interplay between the system's geometry and heat sensitivity.

3. Discussion

While previous work by Wen et al. [16] and AL-Taie [18] has focused on improving thermal performance using core structures filled with fluids or phase-change materials, this study presents a fundamentally different design methodology. Our design is based on a solid silica core structure combined with selective light coloring on the outer surfaces. This simple and robust construction achieves efficient thermal control for heat dissipation, with a significant reduction in thermal and light loss compared to designs with internal fillers or moving fluids. Therefore, the proposed approach offers a more stable and less complex practical solution for maintaining efficiency under extended operating conditions, while avoiding the challenges associated with leakage or degradation of the filling materials.

Two important effects were investigated in this study:

3) The effect of hole diameter (d) on dispersion properties:

It was observed that increasing the hole diameter from 1.5 to 4.5 μm resulted in a decrease in the fundamental ZDW from 1.1324 to 1.0216 μm at 15 °C and an increase in the maximum positive dispersion from 38.67 to 53.24 ps/nm/km. Fibers with larger holes (such as 4.5 μm) exhibited a wider dispersion range, while smaller fibers (1.5 μm) were more sensitive to thermal changes.

The physical explanation for this phenomenon is that increasing the hole diameter reduces the effect of waveguide dispersion

Table 1
Effect of gap diameter on maximum and minimum dispersion at various temperatures

Hole diameter (μm)	ZDW at 15 °C (μm)	ZDW at 95 °C (μm)	ΔZDW (nm)	Min dispersion	Max dispersion
1.5	1.1324	1.1689	36.5	–42.15	38.67
2.5	1.0873	1.1238	36.5	–38.92	45.31
3.5	1.0542	1.0907	36.5	–35.74	49.88
4.5	1.0216	1.0581	36.5	–32.15	53.24

Figure 5
Temperature-dependent dispersion characteristics for PCF with lattice constant K = 3 µm and hole diameters (a) d = 1.5 µm, (b) d = 2.5 µm, (c) d = 3.5 µm, and (d) d = 4.5 µm

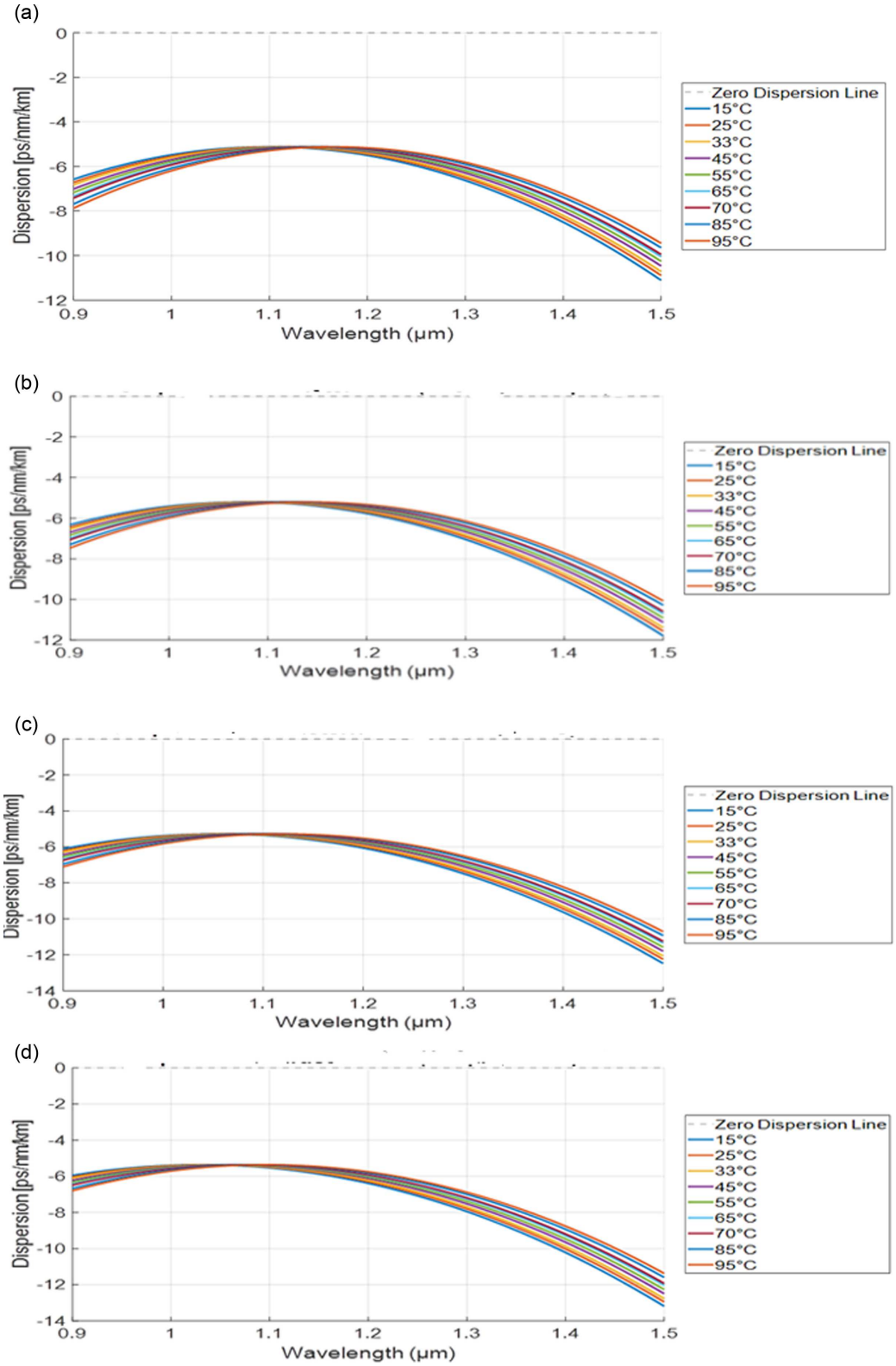

Figure 6
ZDW shift vs PCF temperature with various water-penetrated hole sizes and lattice constant K = 3 µm

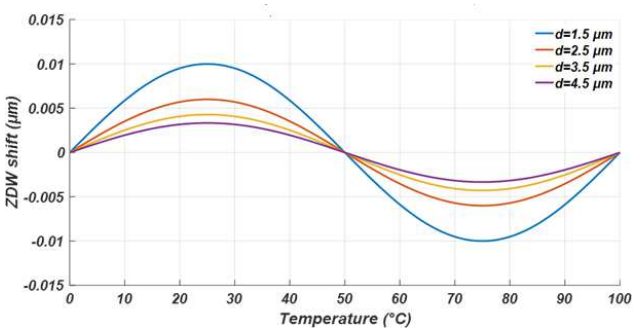

due to reduced interaction between light and the crystal structure, which increases the dominance of material dispersion resulting from water and glass. This shifts the total dispersion toward higher positive values, which explains the increase in maximum dispersion.

4) Effect of temperature on ZDW:

Increasing the temperature from 15 °C to 95 °C caused the ZDW to shift toward longer wavelengths by 36.5 nm for all hole diameters. ZDW accuracy of up to ±5 nm was achieved across a temperature range of 80 °C. The physical explanation for these results is that the decrease in water density with increasing temperature leads to a decrease in its refractive index (according to the equation presented in the research), which alters the balance between material and wave scattering. This change shifts the ZDW toward longer wavelengths, a behavior consistent with thermo-optic models.

The mathematical model used (including the water refractive index equation based on (λ, T, and p) showed remarkable agreement with the numerical results, confirming the effectiveness of the finite element method in modeling complex systems such as liquid-filled PCFs. However, the model could be improved in the future by incorporating pressure and humidity effects. The results of the ZDW transformation with temperature (36.5 nm) are consistent with the work of Park et al. [15] and Karasawa [17], but this study has an improved accuracy (±5 nm) due to the use of improved fiber designs and dynamic thermal control systems (such as Peltier elements). In contrast to studies that focused on liquid-filled cores, this research focused on water penetration into the photosphere, minimizing optical losses due to water absorption at 1.1–1.3 µm. "As a practical consideration, relying on an internal water layer may make the structure sensitive to changes in relative humidity or evaporation rate over the long term. This challenge could be addressed in the future through strategies such as developing nanoscale barrier coatings or using fluids with extremely low vapor pressure to enhance stability in diverse operating environments."

4. Conclusions

The ordered oscillatory behavior of the ZDW shift with temperature demonstrates the potential for intelligent dynamic tuning of optical fiber systems. The dispersive zero point (ZDW)—a critical parameter in broadband communications—can be precisely controlled by adjusting the water temperature within the fiber pores. Each curve represents a ready-made tuning map showing the exact amount of shift expected for each temperature change. The regular decrease in oscillation amplitude with increasing pore diameter (d) highlights a meaningful design differentiation: small-pore (1.5 µm) fibers with high amplitude are suitable as highly sensitive optical thermal sensors or fine-tuning elements, while large-pore (4.5 µm) fibers with limited amplitude offer superior thermal stability and a wider operational range, making them ideal for critical communication systems requiring high tolerance to fluctuations. The design of the water-filled casing system (rather than the core) achieves an ideal balance: it allows sufficient interaction between light and the thermally controlled medium (water) across its no-load field, while significantly reducing optical loss because the underlying glass core remains intact, thus maintaining efficient light transmission. This makes the system practical and manufacturable, as the water-treated fiber segments can be seamlessly integrated into conventional fiber networks as thermally programmable smart photodetectors or photoprocessors.

Ethical Statement

This study does not contain any studies with human or animal subjects performed by any of the authors.

Conflicts of Interest

The authors declare that they have no conflicts of interest to this work.

Data Availability Statement

Data sharing is not applicable to this article as no new data were created or analyzed in this study.

Author Contribution Statement

Mohammed Salim Jasim AL-Taie: Conceptualization, Software, Investigation, Data curation, Writing – original draft, Supervision. **Hayder Ahmed Hasan:** Methodology, Validation, Resources, Project administration. **Mohammed Kadhum Hamad:** Formal analysis, Writing – review & editing, Visualization.

References

[1] Mohammed, N. A., Khedr, O. E., El-Rabaie, E.-S. M., & Khalaf, A. A. M. (2022). Literature review: On-chip photonic crystals and photonic crystal fiber for biosensing and some novel trends. *IEEE Access*, *10*, 47419–47436. https://doi.org/10.1109/ACCESS.2022.3170912

[2] Gangwar, R. K., Pathak, A. K., & Kumar, S. (2023). Recent progress in photonic crystal devices and their applications: A review. *Photonics*, *10*(11), 1199. https://doi.org/10.3390/photonics10111199

[3] Jasim, M. S. (2023). Effect of some parameters on optical soliton pulses in photonic crystal fibers. *Current Applied Science and Technology*, *23*(5), 1–10. https://doi.org/10.55003/cast.2023.05.23.005

[4] Yin, Z., Jing, X., Feng, Y., Gao, Z., Wu, B., & Wang, C. (2022). Refractive index and temperature dual parameter sensor based on a twin-core photonic crystal fiber. *Journal of Physics D: Applied Physics*, *55*(15), 155108. https://doi.org/10.1088/1361-6463/ac472b

[5] Salem, S. S., Hammad, E. N., Mohamed, A. A., & El-Dougdoug, W. (2023). A comprehensive review of nanomaterials: Types, synthesis, characterization, and applications. *Biointerface Research in Applied Chemistry*, *13*(1), 41. https://doi.org/10.33263/BRIAC131.041

[6] Jain, S., Choudhary, K., & Kumar, S. (2022). Photonic crystal fiber-based SPR sensor for broad range of refractive index sensing applications. *Optical Fiber Technology*, *73*, 103030. https://doi.org/10.1016/j.yofte.2022.103030

[7] Sylvestre, T., Genier, E., Ghosh, A. N., Bowen, P., Genty, G., Troles, J., & Dudley, J. M. (2021). Recent advances in supercontinuum generation in specialty optical fibers. *Journal of the Optical Society of America B*, *38*(12), F90–F103. https://doi.org/10.1364/JOSAB.439330

[8] Miah, M. R., Dong, Y., Wang, J., & Zhu, J. (2024). Recent progress on sustainable 2, 5-furandicarboxylate-based polyesters: Properties and applications. *ACS Sustainable Chemistry & Engineering*, *12*(8), 2927–2961. https://doi.org/10.1021/acssuschemeng.3c06878

[9] Butt, M. A., & Khonina, S. N. (2024). Recent advances in photonic crystal and optical devices. *Crystals*, *14*(6), 543. https://doi.org/10.3390/cryst14060543

[10] Maidi, A. M., Abas, P. E., Petra, P. I., Kaijage, S., Zou, N., & Begum, F. (2021). Theoretical considerations of photonic crystal fiber with all uniform-sized air holes for liquid sensing. *Photonics*, *8*(7), 249. https://doi.org/10.3390/photonics8070249

[11] Cai, Z., Li, Z., Ravaine, S., He, M., Song, Y., Yin, Y., & Zhang, A. (2021). From colloidal particles to photonic crystals: Advances in self-assembly and their emerging applications. *Chemical Society Reviews*, *50*(10), 5898–5951. https://doi.org/10.1039/D0CS00706D

[12] Hanoon, R. A., Abdulhadi, A. H., & Abass, A. K. (2025). Design of high nonlinear photonic crystal fiber for ultrashort pulse laser generation. *Journal of Optical Communications*. https://doi.org/10.1515/joc-2024-0209

[13] Scheibinger, R., Hofmann, J., Schaarschmidt, K., Chemnitz, M., & Schmidt, M. A. (2023). Temperature-sensitive dual dispersive wave generation of higher-order modes in liquid-core fibers. *Laser & Photonics Reviews*, *17*(1), 2100598. https://doi.org/10.1002/lpor.202100598

[14] Thi, T. N., Trong, D. H., & van, L. C. (2023). Supercontinuum generation in ultra-flattened near-zero dispersion PCF with C7H8 infiltration. *Optical and Quantum Electronics*, *55*(1), 93. https://doi.org/10.1007/s11082-022-04351-x

[15] Park, K. I., Park, M., & James. (2018). *Fundamentals of probability and stochastic processes with applications to communications*. Germany: Springer International Publishing. https://doi.org/10.1007/978-3-319-68075-0

[16] Wen, J., Liang, B., Qin, W., Sun, W., He, C., & Xiong, K. (2022). High coherent supercontinuum generation in nitrobenzene liquid-core photonic crystal fiber with elliptical air-hole inner ring. *Optical and Quantum Electronics*, *54*(12), 817. https://doi.org/10.1007/s11082-022-04234-1

[17] Karasawa, N. (2012). Dispersion properties of liquid-core photonic crystal fibers. *Applied Optics*, *51*(21), 5259–5265. https://doi.org/10.1364/AO.51.005259

[18] AL-Taie, M. S. J. (2024). Bright and dark soliton pulse in solid core photonic crystal fibers. *Journal of Optics and Photonics Research*, *1*(1), 23–31. https://doi.org/10.47852/bonviewJOPR32021585

[19] Chemnitz, M., Junaid, S., & Schmidt, M. A. (2023). Liquid-core optical fibers—A dynamic platform for nonlinear photonics. *Laser & Photonics Reviews*, *17*(9), 2300126. https://doi.org/10.1002/lpor.202300126

[20] Fuad, M. H., Nayan, M. F., & Mahmud, R. R. (2025). Advances in surface plasmon resonance-based PCF and MIM sensors. *Plasmonics*, *20*(9), 7995–8026. https://doi.org/10.1007/s11468-025-02796-w

[21] Chen, D., Tan, F., Zhang, Z., Zhang, Y., Ge, S., Zhang, X., & Leng, Z. (2025). Design and optimization of a large mode field, low crosstalk homogeneous six-core photonic crystal fiber. *Journal of Non-Crystalline Solids*, *651*, 123383. https://doi.org/10.1016/j.jnoncrysol.2024.123383

[22] Tomer, D. S., & Kumar, A. (2024). Ethanol-infiltrated circular photonic crystal fiber for low peak power supercontinuum generation from near-infrared to mid-infrared region. *Journal of Optics*. https://doi.org/10.1007/s12596-024-02152-x

[23] Li, Y.-L., Liu, K., Wu, H.-M., & Lv, J.-A. (2025). Photonic fibrous liquid crystal elastomer actuators. *Chinese Journal of Polymer Science*, *43*(4), 597–604. https://doi.org/10.1007/s10118-025-3286-x

[24] Blagojevič, M., Hočevar, M., Bizjan, B., Drešar, P., Kolbl Repinc, S., & Rak, G. (2024). Three-dimensional numerical simulation of a two-phase supercritical open channel junction flow. *Water*, *16*(12), 1757. https://doi.org/10.3390/w16121757

[25] Sultana, N., & Islam, M. S. (2026). Comparative investigation of group velocity dispersion with nonlinear phase modulation in fiber optic WDM transmission. *International Journal of Information Technology*, *18*(1), 417–426. https://doi.org/10.1007/s41870-024-02145-w

[26] Butt, M. A., Kazanskiy, N. L., & Khonina, S. N. (2020). Modal characteristics of refractive index engineered hybrid plasmonic waveguide. *IEEE Sensors Journal*, *20*(17), 9779–9786. https://doi.org/10.1109/JSEN.2020.2991215

[27] AL-Taie, M. S. J. (2024). Optimal integrating techniques for supercontinuum simulations. *Indian Journal of Physics*, *98*(10), 3593–3599. https://doi.org/10.1007/s12648-024-03108-4

How to Cite: Salim Jasim AL-Taie, M., Hasan, H. A., & Hamad, M. K. (2026). Effect of Temperature on the Dispersion Properties of Water-Filled Photonic Crystal Fibers. *Journal of Optics and Photonics Research*. https://doi.org/10.47852/bonviewJOPR62027923